Multimodal Imaging of Biological Tissues Using Combined MALDI and NAPA-LDI Mass Spectrometry for Enhanced Molecular Coverage

Journal:	*Analyst*
Manuscript ID	AN-ART-04-2020-000836.R1
Article Type:	Paper
Date Submitted by the Author:	09-Jul-2020
Complete List of Authors:	Fincher, Jarod; George Washington University, Department of Chemistry Korte, Andrew; George Washington University, Department of Chemistry Yadavilli, Sridevi; Children's National Medical Center, Research Center for Genetic Medicine Morris, Nicholas; UES Inc Vertes, Akos; George Washington University, Department of Chemistry

Multimodal Imaging of Biological Tissues Using Combined MALDI and NAPA-LDI Mass Spectrometry for Enhanced Molecular Coverage

Jarod A. Fincher[1], Andrew R. Korte*[1], Sridevi Yadavilli[2], Nicholas J. Morris[3], and Akos Vertes*[1]

[1]*Department of Chemistry, The George Washington University, Washington, DC 20052, USA*

[2]*Research Center for Genetic Medicine, Children's National Medical Center, Washington, DC 20010, USA*

[3]*UES, Inc., Beavercreek, OH 45432, USA*

*Co-corresponding authors:

Akos Vertes

Email: vertes@gwu.edu

ORCID: 0000-0001-5186-5352

Andrew Korte

Email: andrew.r.korte@gmail.com

ORCID: 0000-0003-4270-966X

Mass spectrometry imaging (MSI) is a powerful analytical technique that enables detection, discovery, and identification of multiple classes of biomolecules, while simultaneously mapping their spatial distributions within a sample (e.g., a section of biological tissue). The limitation in molecular coverage afforded by any single MSI platform has led to the development of multimodal approaches that incorporate two or more techniques to obtain greater chemical information. Matrix-assisted laser desorption ionization (MALDI) is a preeminent ionization technique for MSI applications because the wide range of available matrices allows some degree of enhancement with respect to the detection of particular molecular classes. Nonetheless, MALDI has a limited ability to detect and image several classes of molecules, e.g., neutral lipids, in complex samples. Laser desorption ionization from silicon nanopost arrays (NAPA-LDI or NAPA) has been shown to offer complementary coverage with respect to MALDI by providing improved detection of neutral lipids and some small metabolites. Here, we present a multimodal imaging method in which a single tissue section is consecutively imaged at low and high laser fluences, generating spectra that are characteristic of MALDI and NAPA ionization, respectively. The method is demonstrated to map the distributions of species amenable to detection by MALDI (e.g., phospholipids and intermediate-mass metabolites) and NAPA (e.g., neutral lipids such as triglycerides and hexosylceramides, and small metabolites) in mouse brain and lung tissue sections.

1. Introduction

Mass spectrometry imaging (MSI) is becoming a useful tool in histology and drug discovery due to its ability to spatially map diverse biomolecules, including metabolites, lipids, peptides, and proteins, in tissue sections without the need for chemical labeling.[1-5] For example, MSI has been used for the classification of tumor subtypes, and to identify tumor margins between cancerous and noncancerous tissue regions.[6-10] In addition, spatial mapping of drug candidates, pharmaceuticals and the corresponding metabolites has been demonstrated, even achieving absolute quantitation in some cases.[11-14] Currently, matrix-assisted laser desorption ionization (MALDI) is a top method for MSI due to its relative simplicity, broad molecular coverage, and wide availability of the required instrumentation. The impressive molecular coverage provided by MALDI can, in part, be attributed to the large array of available matrices, with many of them providing preferential ionization of different biomolecular classes.[15-17]

While MSI provides detailed chemical information, in most configurations it cannot match the spatial resolution afforded by optical microscopy. Moreover, the chemical information provided by an MSI experiment varies significantly depending upon the chosen sample preparation and ionization technique. To overcome these limitations, methodologies have been developed in which two or more imaging techniques are combined to provide complementary information. In the most common implementation of this approach, a tissue section is collected from the region immediately adjacent to the section subjected to MSI, and is designated for histological staining, e.g., by hematoxylin and eosin (H&E), and imaging by optical microscopy. Image fusion allows for the combination of optical images of histologically stained tissues (high spatial resolution and low chemical specificity) with MSI-generated chemical images (lower spatial resolution and high chemical specificity) to infer molecular distributions at higher spatial resolutions than typically achieved by MSI alone.[18] Considerable effort is being directed toward developing multimodal imaging platforms that combine two or more MSI ionization modalities. For example, MALDI has been combined with secondary ion mass spectrometry (SIMS) or desorption electrospray ionization (DESI), and imaging of the same tissue section by MALDI in positive and negative ion mode has been demonstrated.[19-21] MALDI-MSI images have also been co-registered with autofluorescence and magnetic resonance imaging (MRI) to provide complementary information.[22, 23]

Although MALDI offers excellent molecular coverage in MSI, in complex samples it exhibits low ionization efficiency for some small metabolites and for neutral lipids, such as triglycerides (TGs) and hexosylceramides (HexCers). The detection of neutral lipids is hindered by ion suppression effects induced by phospholipids, for example, phosphatidylcholines (PCs).[24-26] To circumvent these limitations, several novel LDI methods utilizing a large variety of nanomaterials and nanostructures have been developed.[27] For example, silver or gold nanoparticles provide remarkably higher ionization efficiencies for TGs.[28-31] In the recently developed MALDI-2 technique, a second laser intercepts the desorption plume for post-ionization, resulting in significantly enhanced sensitivity and the detection of less abundant species. This was shown to greatly improve the molecular coverage of neutral lipid species and phospholipids, as well as often difficult to detect sterols and pharmaceuticals.[32-35]

Comparing MALDI with LDI from silicon nanopost arrays (NAPA),[36] a matrix-free MS platform, has been shown to provide complementary coverage for metabolites.[37, 38] Molecular imaging of biological samples has also been demonstrated by NAPA-MSI.[39] A remarkable difference between the fluence dependence of the two ionization methods is the significantly lower ionization threshold for MALDI compared to LDI from NAPA.[40] This presents an opportunity for the combination of these two techniques to study the same tissue section by both MSI modalities. Compared to MALDI, enhanced ionization efficiency was observed by LDI from NAPA for neutral lipid classes such as TGs and HexCers, whereas for phospholipids MALDI exhibited higher ion yields.[41-43] Thus, a combined method is expected to provide broader molecular coverage compared to the two techniques performed separately.

Here we present a new multimodal imaging approach that combines the ionization capabilities afforded by the MALDI- and NAPA-LDI-MSI platforms to obtain improved molecular coverage in imaging of a single tissue section (see Figure 1). This is made possible, in large part, by the significantly different laser fluence needed for ion production by the two platforms. For the combined technique, a tissue section is thaw-mounted on top of the nanofabricated silicon posts in the NAPA chip, and a thin layer of MALDI matrix is applied to the surface of this sample. In the first MSI pass, a relatively low laser fluence is applied to generate MALDI spectra. At this laser fluence the NAPA structure below the tissue section does not contribute to ion production. In the second MSI pass, a comparatively high laser fluence is applied to deposit enough energy into the underlying nanoposts to induce desorption and ionization. The utility of the combined method is demonstrated on MSI of mouse brain and lung tissue sections.

2. Experimental

2.1 Chemicals

Solvents methanol (catalog no. A452-4) and water (catalog no. W6-212) were purchased at LC-MS grade from Fisher Scientific (Hampton, NH). Matrices 9-aminoacridine (9-AA, catalog no. 92817) and α-cyano-4-hydroxycinnamic acid (CHCA, catalog no. C8982) for MALDI were purchased from Sigma-Aldrich (St. Louis, MO).

2.2 Fabrication of NAPA Imaging Chips

The detailed process for the nanofabrication of NAPA imaging chips has been described in a previous publication.[44] Briefly, silicon nanoposts were produced with a periodicity of 337 nm and post dimensions of 1100 nm in height and 150 nm in diameter optimized for maximum ion yield by LDI. NAPA imaging chips were fabricated from low-resistivity p-type silicon wafers (Silicon Valley Microelectronics, Inc., Santa Clara, CA) by methods utilizing deep ultraviolet projection lithography (DUV-PL) followed by deep reactive ion etching (DRIE). The size of a typical imaging NAPA chip was 25 × 25 mm^2.

2.3 Sample Preparation for MSI

Whole mouse brains and mouse lungs were provided by Children's National Medical Center (Washington, DC) in accordance with the protocol approved by the Institutional Animal Care and Use Committee (IACUC). All tissue samples were stored at -80 °C until preparation for MSI analysis, whereupon they were placed into a pre-chilled cryomicrotome (CM1800, Leica Microsystems Inc., Nussloch, Germany) at -25 °C and allowed to equilibrate for 30 min before sectioning. Both mouse brain and mouse lung tissue samples were sectioned at 10 µm thickness and immediately thaw-mounted onto NAPA imaging chips and placed in a vacuum desiccator for 30 min.

Matrix deposition was performed using an in-house built oscillating capillary nebulizer. Briefly, an Aztek A470 airbrush (Testors, Vernon Hills, IL) was modified to accommodate a fused silica capillary threaded through the spray nozzle. Matrix solution was fed through the capillary by means of a syringe (1750TLL, Hamilton Co., Reno, NV) and a syringe pump (KS100, KD Scientific, Holliston, MA). The airbrush nozzle was positioned ~23 cm above the tissue surface and spraying was driven by nitrogen as the nebulizing gas at a pressure of 276 kPa (40 psi). For lung imaging experiments, a 20 mg/mL solution of CHCA in methanol was sprayed at a flow rate of 50 µL/min, with a total sprayed volume of 300 µL. For brain imaging experiments, a 10 mg/mL solution of 9-AA in methanol was sprayed at 50 µL/min, with a total sprayed volume of 300 µL.

2.4 Data Acquisition and Analysis

All MSI data for mouse brain and mouse lung tissue samples were acquired on a MALDI-LTQ-Orbitrap XL mass spectrometer equipped with a nitrogen laser emitting radiation at 337 nm with a 60 Hz repetition rate and a focal spot size of ~80 µm × 100 µm (Thermo Scientific, San Jose, CA). The laser was operated at fluences in the 40-50 mJ/cm^2 range with 10 shots/scan for MALDI (MALDI pass) and in the 140-200 mJ/cm^2 range with 3 shots/scan for NAPA (NAPA pass). In the MALDI pass most of the matrix material was removed from the tissue surface at the focal spot. Thus, in the MALDI pass, no ions were generated by LDI from NAPA, and in the NAPA pass, ion production was dominated by the NAPA-LDI process. Imaging data was collected with a modest lateral resolution of 100 µm, well below what was achievable by either of the methods.[39] All MSI experiments were run at a mass resolving power setting of 30,000 with an *m/z* range of 500 to 1,000. Reproducibility of NAPA-LDI-MSI has been demonstrated for biological applications, including the same type of mouse brain and lung tissues.[41, 43] Well-controlled matrix application is a critical factor for reproducible MALDI-MSI. It is achievable by several matrix application methods, including the one used in this study.[45]

All imaging data were processed by importing the raw data files (*.raw) into ImageQuest (Thermo Scientific, San Jose, CA), whereby chemical images were generated with a mass tolerance of ≤ 5 mDa. In order to co-register the chemical images generated by the MALDI pass and the NAPA pass, chemical images were exported out of ImageQuest and imported into ImageJ, a freely available image processing software.[46] The images were then overlaid using the alignment of two color channels. Lipid ions were tentatively identified by matching measured *m/z* values to a previously assembled in-house reference list with mass accuracy tolerance of $\Delta m/z \leq \pm 5$ mDa. For mouse brain and lung tissues, this list had been compiled based on UPLC-MS/MS measurements.[41, 43] Putative lipid assignments for this work can be found in the Electronic Supplementary Information.

3. Results and discussion

To demonstrate multimodal imaging using the combination of MALDI and NAPA-LDI, a 10 µm thick mouse brain tissue section was thaw-mounted onto a NAPA imaging chip and placed in a vacuum desiccator for ~30 min. The dehydrated tissue section was spray coated by 9-AA matrix using the oscillating capillary nebulizer built in house. First, MALDI-MSI was performed at a low laser fluence

(~40 mJ/cm^2) in negative ion mode, allowing detection and imaging of lipid classes such as sulfatides (STs) and phosphatidylinositols (PIs) (see the top image panels in Figure 2). The number of laser pulses for each spot in this MALDI pass was selected to remove most of the matrix material from the tissue surface. Observing the depletion of the matrix signal indicated that ten laser pulses per spot was sufficient to achieve this condition. In general, this number depends on the nature of the matrix and the applied laser fluence. In the MALDI pass, medium-size metabolites including UDP-ribose, ADP-ribose, and oxidized glutathione were also detected. Immediately upon the completion of the MALDI imaging acquisition, the same tissue section was re-imaged in positive ion mode at a considerably higher laser fluence (~160 mJ/cm^2) by NAPA-LDI, whereby phosphatidylethanolamines (PEs), phosphatidylethanolamine plasmalogens (PEps), and HexCers among other molecular species were selectively ionized and detected (see image panels in the middle in Figure 2). Comparison of the integrated mass spectra for the MALDI pass and the NAPA pass in the bottom panel of Figure 2 illustrates the complementary nature of the two ionization techniques. An extensive tentative identification list for the detected ions in mouse brain tissue section is presented in Table S1 of the Electronic Supplementary Information.

The complementary molecular coverages of these two platforms have been evaluated and discussed in detail in previous work.[37, 41, 43] In brief, unlike MALDI, NAPA has been shown to efficiently ionize neutral lipid species, such as HexCers TGs, as well as PE plasmalogens. In contrast, MALDI has been proven superior at efficiently ionizing phospholipid species, such as PCs and SMs in positive ion mode, as well as STs and PIs in negative ion mode. Additionally, the lower internal energy of MALDI-generated ions is more conducive for the detection of thermally labile compounds like ADP-ribose and glutathione. Indeed, whereas MALDI generates ions with lower but matrix dependent internal energy, the ions produced from NAPA exhibit a higher, laser fluence and polarization dependent internal energy.[47, 48]

The ability to reimage the same tissue by the two ionization techniques relies on the observation that laser exposure in MALDI only consumes the matrix material and does not remove most of the underlying tissue. As the matrix solution droplets are deposited on the sample surface, they dissolve some components of the tissue and upon drying matrix-analyte co-crystallization occurs. Laser exposure of these crystals in the MALDI pass gives rise to the MALDI signal, and upon multiple exposures the matrix crystals are almost completely removed from the interrogated tissue surface. In the NAPA pass, the laser radiation traverses through the exposed tissue and the underlying silicon nanoposts absorb the laser pulse energy. The rapidly heating nanoposts induce the volatilization of the tissue at the tips of the posts, and field enhancement at these same tips results in efficient ionization.

Additional capabilities of the combined MALDI and NAPA-LDI MSI method were tested on an alternative tissue sample. A 10-μm thick mouse lung tissue section was thaw-mounted onto a NAPA imaging chip as described above. The tissue was coated with CHCA MALDI matrix. In a departure from the brain imaging experiments, the lung tissue was imaged in positive ion mode by both techniques. First, MALDI-MSI was performed at a lower laser fluence (~40 mJ/cm^2). This was immediately followed by re-imaging of the same tissue section at higher laser fluence (~200 mJ/cm^2) by NAPA-LDI. As seen in Figure 3, phospholipids such as phosphatidylcholines (PCs) were selectively ionized in the MALDI pass at reduced laser fluence. When re-imaging the same tissue at higher laser fluence in the NAPA pass, TGs and PEs were selectively ionized. A tentative identification list for the detected ions in the mouse lung tissue section is presented in Table S2 of the Electronic Supplementary Information.

To demonstrate the complementary nature of the two imaging modalities, MALDI and NAPA-LDI images are compared for the same ions in the top and middle row of panels in Figure 3, respectively.

Distributions for PC ions at *m/z* 756.558 ([PC(34:3)+H]$^+$) and *m/z* 780.553 ([PC(36:5)+H]$^+$) are clearly revealed by the MALDI pass (see the two left panels in the top row in Figure 3), whereas the NAPA pass (see the two left panels in the middle row in Figure 3) does not provide discernable patterns. Conversely, for *m/z* 780.496 ([PE(36:3)+K]$^+$) and *m/z* 879.742 ([TG(52:3)+Na]$^+$) the MALDI pass resulted in week to no signal (see the two right panels in the top row in Figure 3), whereas the NAPA pass produced detailed distributions (see the two right panels in the middle row in Figure 3).This complementarity is also illustrated by the mass spectra integrated for the MALDI and NAPA-LDI images (see the bottom panel in Figure 3).

As seen in Figure 4, the acquisition of MALDI and NAPA images from the same tissue section allows for detection and imaging of lipid classes that are not typically detected using a single MSI platform or ion polarity. This circumvents the need for the preparation of multiple consecutive sample sections, eliminating concerns about variability in sample treatment and tissue heterogeneity. Given the incompatibility of MS imaging with typical tissue fixation techniques, preparation of highly similar consecutive sections is non-trivial. Moreover, the typical tissue section thickness (~10 µm) is on the order of the size of most animal cells, so the chemical similarity of consecutive sections cannot be assured.

The use of the same tissue section for the two techniques also simplifies image processing. In these experiments, imaging in both modalities was performed using the same instrument position file and there was no need to identify fiducial markers for coregistration. In the brain imaging presented here, overlaying images for *m/z* 885.550 (detected by negative ion mode MALDI and identified as [PI(38:4)-H]$^-$) and *m/z* 866.645 (detected by positive ion mode NAPA and identified as [HexCer(t42:1)+K]$^+$) revealed complementary distributions, with localization to the gray and white matter, respectively. Similarly, *m/z* 888.625 (MALDI, identified as [ST(d42:2)-H]$^-$) localized to the white matter and *m/z* 852.467 (NAPA, identified as [PEp(40:6)+2K-H]$^+$) localized to the gray matter were found to have complementary spatial distributions. Overlaying cross-platform lung tissue images also revealed complementary localizations among PCs, TAGs, and PEs (see Figure S1 in the Electronic Supplementary Information).

The ability of the dual imaging platform presented here to detect a range of biomolecules presents numerous potential applications. For example, many of the species shown in Figures 2, 3 and 4 are implicated in important biological processes or disease progression. Reduced glutathione (shown in its oxidized form (GSSG) in the top panel of Figure 2) is the predominant antioxidant in brain tissue, and plays a crucial role in protecting nervous tissue from oxidative damage that has been implicated in neurological diseases such as Alzheimer's disease and Parkinson's disease.[49] Furthermore, PE lipids have been shown to be associated with Alzheimer's disease, where they were found to be significantly decreased in diseased tissue.[50] ADP-ribose (see its distribution in the top panel in Figure 2) is known to be involved in repair of DNA damage.[51] Within the brain, sulfatides (distributions are shown in the middle and top panels of Figure 2 and the left panel of Figure 4) and HexCers (see distributions in the middle panel of Figure 2 and the center panel of Figure 4) are critical to the development of the myelin sheath. They also factor into many forms of extracellular binding, including bacterial and viral infection.[52] PIs (demonstrated in the top and left panels of Figures 2 and 4, respectively) exist in a vast multitude of forms and isomers, and a recent review has extensively discussed their roles in cellular signaling and disease.[53] In breast cancer tissue samples, PCs (examples are depicted in the top panel of Figure 3) were detected at significantly higher levels, allowing for differentiation between cancerous and non-cancerous tissue types.[54] Lastly, increased levels of TGs (shown in the middle panel of Figure 3) have been associated with life-altering diseases like type-2 diabetes and coronary heart disease.[55-57]

4. Conclusions

The multimodal imaging platform based on the combination of MALDI and NAPA-LDI has been demonstrated for imaging of chemical species in mouse brain and lung tissues and can be applied to other sample types. In these experiments, the consecutive use of MALDI- and NAPA-LDI-MSI allowed for the detection and imaging of a range of chemical species, including several classes of lipids and small molecule metabolites. Although the high fluences required for NAPA-LDI-MSI are typically destructive to the tissue sample, we envision that multiple MALDI imaging analyses (e.g. in different polarities) can be performed prior to a final NAPA-LDI-MSI step. This dual imaging capability offers enhanced molecular coverage in MSI experiments, providing enriched information on spatial variations or temporal changes in lipid composition. For example, this multimodal imaging platform could be used to investigate host-pathogen interactions, an area of research where MSI has already provided insight into inflammatory signaling pathways with respect to lipids and microbial pathogenesis.[58, 59]

Acknowledgement

Research was sponsored by the U.S. Army Research Office and the Defense Advanced Research Projects Agency and was accomplished under Cooperative Agreement Number W911NF-14-2-0020. The views and conclusions contained in this document are those of the authors and should not be interpreted as representing the official policies, either expressed or implied, of the Army Research Office, DARPA, or the U.S. Government. The U.S. Government is authorized to reproduce and distribute reprints for Government purposes notwithstanding any copyright notation hereon.

The silicon NAPA structures used in this work were produced at the UC Santa Barbara Nanofabrication Facility, a part of the NSF funded National Nanotechnology Infrastructure Network.

Ethical Statement

All experiment were performed in accordance with the guidelines of IACUC and approved by the IACUC.

References

1. R. M. Caprioli, T. B. Farmer and J. Gile, *Anal. Chem.*, 1997, **69**, 4751-4760.
2. R. W. Hutchinson, A. G. Cox, C. W. McLeod, P. S. Marshall, A. Harper, E. L. Dawson and D. R. Howlett, *Anal. Biochem.*, 2005, **346**, 225-233.
3. S. N. Jackson, M. Ugarov, T. Egan, J. D. Post, D. Langlais, J. A. Schultz and A. S. Woods, *J. Mass Spectrom.*, 2007, **42**, 1093-1098.
4. K. Chughtai and R. M. A. Heeren, *Chem. Rev.*, 2010, **110**, 3237-3277.
5. P. Nemes, A. S. Woods and A. Vertes, *Anal. Chem.*, 2010, **82**, 982-988.
6. L. S. Eberlin, I. Norton, A. L. Dill, A. J. Golby, K. L. Ligon, S. Santagata, R. G. Cooks and N. Y. R. Agar, *Cancer Res.*, 2012, **72**, 645-654.
7. S. Santagata, L. S. Eberlin, I. Norton, D. Calligaris, D. R. Feldman, J. L. Ide, X. H. Liu, J. S. Wiley, M. L. Vestal, S. H. Ramkissoon, D. A. Orringer, K. K. Gill, I. F. Dunn, D. Dias-Santagata, K. L. Ligon, F. A. Jolesz, A. J. Golby, R. G. Cooks and N. Y. R. Agar, *Proc. Natl. Acad. Sci. U. S. A.*, 2014, **111**, 11121-11126.

8. S. Kang, H. S. Shim, J. S. Lee, D. S. Kim, H. Y. Kim, S. H. Hong, P. S. Kim, J. H. Yoon and N. H. Cho, *J. Proteome Res.*, 2010, **9**, 1157-1164.
9. P. Chaurand, M. E. Sanders, R. A. Jensen and R. M. Caprioli, *Am. J. Pathol.*, 2004, **165**, 1057-1068.
10. J. Kriegsmann, M. Kriegsmann and R. Casadonte, *Int. J. Oncol.*, 2015, **46**, 893-906.
11. F. P. Y. Barre, M. R. L. Paine, B. Flinders, A. J. Trevitt, P. D. Kelly, R. Ait-Belkacem, J. P. Garcia, L. B. Creemers, J. Stauber, R. J. Vreeken, B. Cillero-Pastor, S. R. Ellis and R. M. A. Heeren, *Anal. Chem.*, 2019, **91**, 10840-10848.
12. J. G. Swales, G. Hamm, M. R. Clench and R. J. A. Goodwin, *Int. J. Mass spectrom.*, 2019, **437**, 99-112.
13. J. M. Wiseman, D. R. Ifa, Y. X. Zhu, C. B. Kissinger, N. E. Manicke, P. T. Kissinger and R. G. Cooks, *Proc. Natl. Acad. Sci. U. S. A.*, 2008, **105**, 18120-18125.
14. B. M. Prentice, C. W. Chumbley and R. M. Caprioli, *J. Am. Soc. Mass. Spectrom.*, 2017, **28**, 136-144.
15. M. C. Fitzgerald, G. R. Parr and L. M. Smith, *Anal. Chem.*, 1993, **65**, 3204-3211.
16. A. Thomas, J. L. Charbonneau, E. Fournaise and P. Chaurand, *Anal. Chem.*, 2012, **84**, 2048-2054.
17. A. R. Buchberger, K. DeLaney, J. Johnson and L. J. Li, *Anal. Chem.*, 2018, **90**, 240-265.
18. R. Van de Plas, J. H. Yang, J. Spraggins and R. M. Caprioli, *Nat. Methods*, 2015, **12**, 366-U138.
19. S. Chughtai, K. Chughtai, B. Cillero-Pastor, A. Kiss, P. Agrawal, L. MacAleese and R. M. A. Heeren, *Int. J. Mass spectrom.*, 2012, **325**, 150-160.
20. L. S. Eberlin, X. H. Liu, C. R. Ferreira, S. Santagata, N. Y. R. Agar and R. G. Cooks, *Anal. Chem.*, 2011, **83**, 8366-8371.
21. S. R. Ellis, J. Cappell, N. O. Potocnik, B. Balluff, J. Hamaide, A. Van der Linden and R. M. A. Heeren, *Analyst*, 2016, **141**, 3832-3841.
22. N. H. Patterson, M. Tuck, R. Van de Plas and R. M. Caprioli, *Anal. Chem.*, 2018, **90**, 12395-12403.
23. A. S. Attia, K. A. Schroeder, E. H. Seeley, K. J. Wilson, N. D. Hammer, D. C. Colvin, M. L. Manier, J. J. Nicklay, K. L. Rose, J. C. Gore, R. M. Caprioli and E. P. Skaar, *Cell Host Microbe*, 2012, **11**, 664-673.
24. G. R. Asbury, K. Al-Saad, W. F. Siems, R. M. Hannan and H. H. Hill, *J. Am. Soc. Mass. Spectrom.*, 1999, **10**, 983-991.
25. B. Emerson, J. Gidden, J. O. Lay, Jr. and B. Durham, *J. Lipid Res.*, 2010, **51**, 2428-2434.
26. M. Petkovic, J. Schiller, M. Muller, S. Benard, S. Reichl, K. Arnold and J. Arnhold, *Anal. Biochem.*, 2001, **289**, 202-216.
27. J. A. Stolee, B. N. Walker, V. Zorba, R. E. Russo and A. Vertes, *PCCP*, 2012, **14**, 8453-8471.
28. M. Dufresne, J. F. Masson and P. Chaurand, *Anal. Chem.*, 2016, **88**, 6018-6025.
29. M. Dufresne, A. Thomas, J. Breault-Turcot, J.-F. Masson and P. Chaurand, *Anal. Chem.*, 2013, **85**, 3318-3324.
30. S. N. Jackson, K. Baldwin, L. Muller, V. M. Womack, J. A. Schultz, C. Balaban and A. S. Woods, *Anal. Bioanal. Chem.*, 2014, **406**, 1377-1386.
31. J. Son, G. Lee and S. Cha, *J. Am. Soc. Mass. Spectrom.*, 2014, **25**, 891-894.
32. J. Soltwisch, H. Kettling, S. Vens-Cappell, M. Wiegelmann, J. Muthing and K. Dreisewerd, *Science*, 2015, **348**, 211-215.
33. S. R. Ellis, J. Soltwisch, M. R. L. Paine, K. Dreisewerd and R. M. A. Heeren, *Chem. Commun.*, 2017, **53**, 7246-7249.
34. M. Niehaus, J. Soltwisch, M. E. Belov and K. Dreisewerd, *Nat. Methods*, 2019, **16**, 925-931.

35. A. P. Bowman, J. F. J. Bogie, J. J. A. Hendriks, M. Haidar, M. Belov, R. M. A. Heeren and S. R. Ellis, *Anal. Bioanal. Chem.*, 2020, **412**, 2277-2289.
36. B. N. Walker, J. A. Stolee, D. L. Pickel, S. T. Retterer and A. Vertes, *J. Phys. Chem. C*, 2010, **114**, 4835-4840.
37. A. R. Korte, N. J. Morris and A. Vertes, *Anal. Chem.*, 2019, **91**, 3951-3958.
38. A. R. Korte, S. A. Stopka, N. Morris, T. Razunguzwa and A. Vertes, *Anal. Chem.*, 2016, **88**, 8989-8996.
39. S. A. Stopka, C. Rong, A. R. Korte, S. Yadavilli, J. Nazarian, T. T. Razunguzwa, N. J. Morris and A. Vertes, *Angew Chem Int Edit*, 2016, **55**, 4482-4486.
40. J. A. Stolee, B. N. Walker, Y. Chen and A. Vertes, in *International Symposium on High Power Laser Ablation 2010*, ed. C. R. Phipps, 2010, vol. 1278, pp. 98-110.
41. J. A. Fincher, J. E. Dyer, A. R. Korte, S. Yadavilli, N. J. Morris and A. Vertes, *J. Comp. Neurol.*, 2019, **527**, 2101-2121.
42. J. A. Fincher, D. R. Jones, A. R. Korte, J. E. Dyer, P. Parlanti, A. Popratiloff, C. A. Brantner, N. J. Morris, R. K. Pirlo, V. K. Shanmugam and A. Vertes, *Sci. Rep.*, 2019, **9**, 17508.
43. J. A. Fincher, A. R. Korte, J. E. Dyer, S. Yadavilli, N. J. Morris, D. R. Jones, V. K. Shanmugam, R. K. Pirlo and A. Vertes, *J. Mass Spectrom.*, 2020, **55**, e4443.
44. N. J. Morris, H. Anderson, B. Thibeault, A. Vertes, M. J. Powell and T. T. Razunguzwa, *RSC Advances*, 2015, **5**, 72051-72057.
45. E. Gemperline, S. Rawson and L. J. Li, *Anal. Chem.*, 2014, **86**, 10030-10035.
46. C. A. Schneider, W. S. Rasband and K. W. Eliceiri, *Nat. Methods*, 2012, **9**, 671-675.
47. G. H. Luo, I. Marginean and A. Vertes, *Anal. Chem.*, 2002, **74**, 6185-6190.
48. J. A. Stolee and A. Vertes, *PCCP*, 2011, **13**, 9140-9146.
49. R. Dringen, *Prog. Neurobiol.*, 2000, **62**, 649-671.
50. R. B. Chan, T. G. Oliveira, E. P. Cortes, L. S. Honig, K. E. Duff, S. A. Small, M. R. Wenk, G. H. Shui and G. Di Paolo, *J. Biol. Chem.*, 2012, **287**, 2678-2688.
51. C. Liu, A. Vyas, M. A. Kassab, A. K. Singh and X. C. Yu, *Nucleic Acids Res.*, 2017, **45**, 8129-8141.
52. T. Takahashi and T. Suzuki, *J. Lipid Res.*, 2012, **53**, 1437-1450.
53. P. Raghu, A. Joseph, H. Krishnan, P. Singh and S. Saha, *Front. Mol. Neurosci.*, 2019, **12**.
54. S. Guenther, L. J. Muirhead, A. V. M. Speller, O. Golf, N. Strittmatter, R. Ramakrishnan, R. D. Goldin, E. Jones, K. Veselkov, J. Nicholson, A. Darzi and Z. Takats, *Cancer Res.*, 2015, **75**, 1828-1837.
55. M. Adiels, S. O. Olofsson, M. R. Taskinen and J. Boren, *Arteriosclerosis Thrombosis and Vascular Biology*, 2008, **28**, 1225-1236.
56. G. S. Berenson, S. R. Srinivasan, W. H. Bao, W. P. Newman, R. E. Tracy, W. A. Wattigney and S. Bogaulas Heart, *New Engl. J. Med.*, 1998, **338**, 1650-1656.
57. M. R. Taskinen, *Diabetologia*, 2003, **46**, 733-749.
58. A. J. Scott, J. M. Post, R. Lerner, S. R. Ellis, J. Lieberman, K. A. Shirey, R. M. A. Heeren, L. Bindila and R. K. Ernst, *Proc. Natl. Acad. Sci. U. S. A.*, 2017, **114**, 12596-12601.
59. J. L. Moore, R. M. Caprioli and E. P. Skaar, *Curr. Opin. Microbiol.*, 2014, **19**, 45-51.

Figures

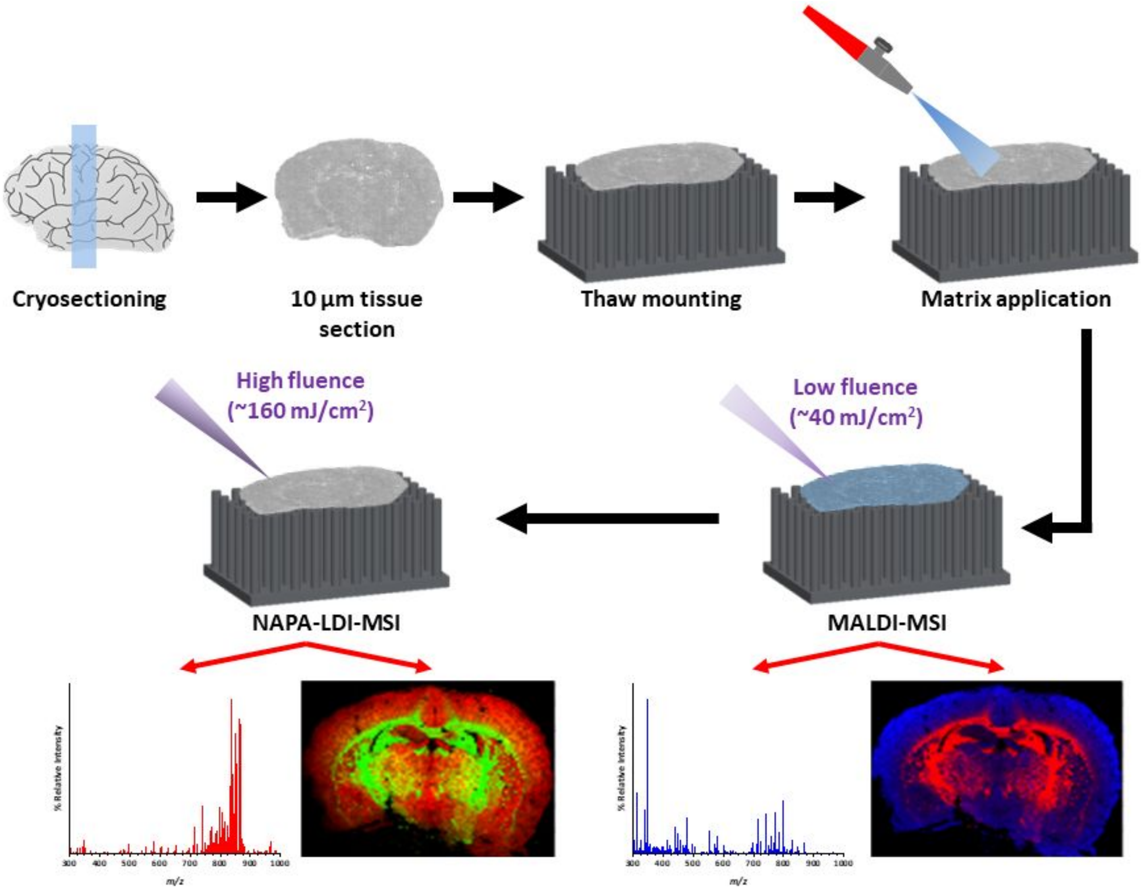

Figure 1. Simplified schematic demonstrating multimodal imaging of a single tissue section by MALDI- and NAPA-LDI-MSI. The MALDI pass is performed at ~40 mJ/cm^2, whereas for the NAPA pass the laser is operated at ~160 mJ/cm^2. Chemical images shown in this illustration present different lipid species detected with similar spatial distributions using the two different platforms and are intended to help illustrate the application workflow.

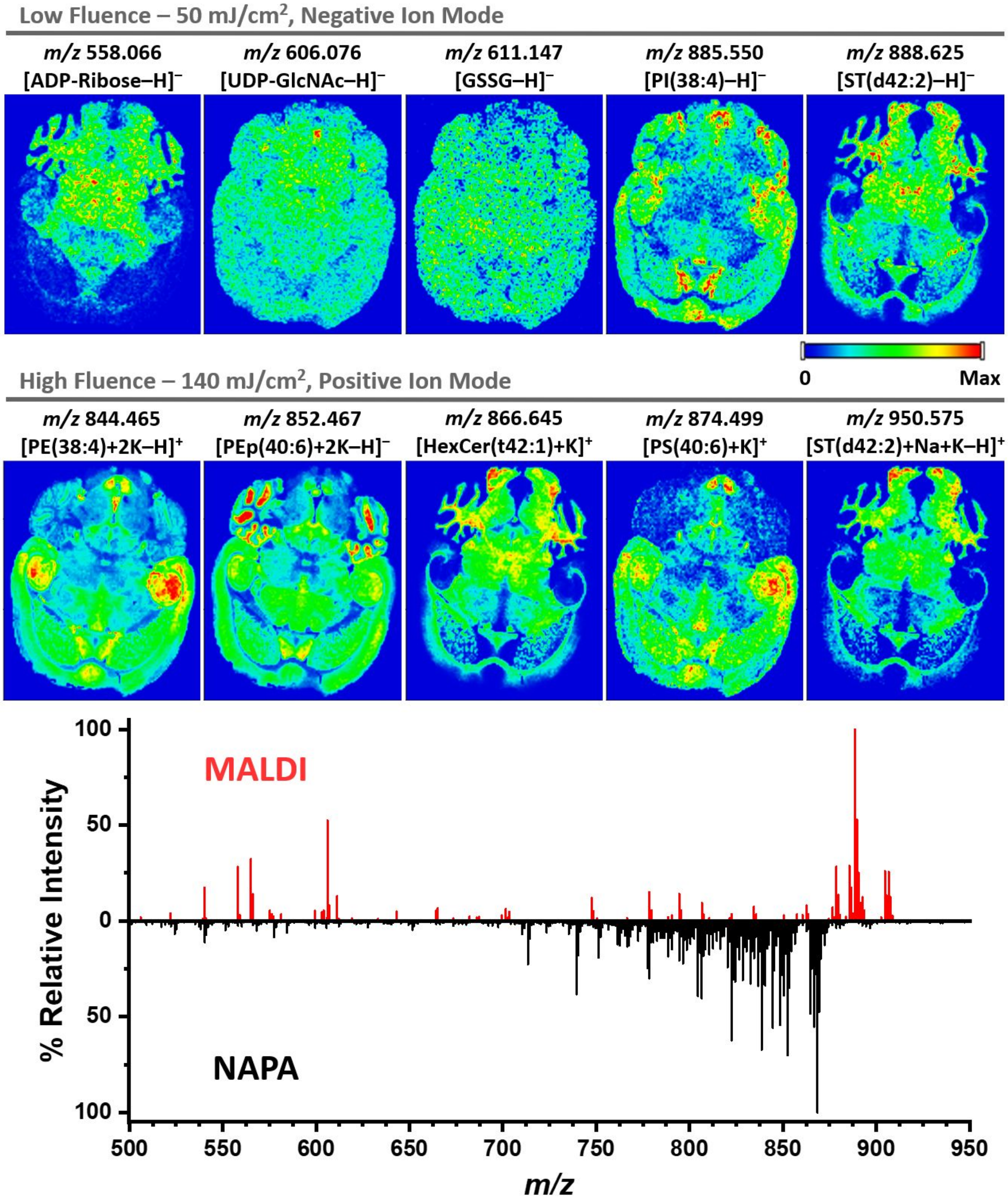

Figure 2. Ion distribution images showing spectral intensities for specific *m/z* values throughout a section of mouse brain tissue. Images at the top were generated from low fluence negative mode data in a MALDI pass, whereas images in middle panels were produced from high fluence positive mode data collected in a NAPA pass. Acquisitions were performed consecutively on the same tissue section. In the bottom panel, comparison of mass spectra is shown averaged over approximately the entire tissue area for the MALDI- and NAPA-LDI-MSI acquisitions.

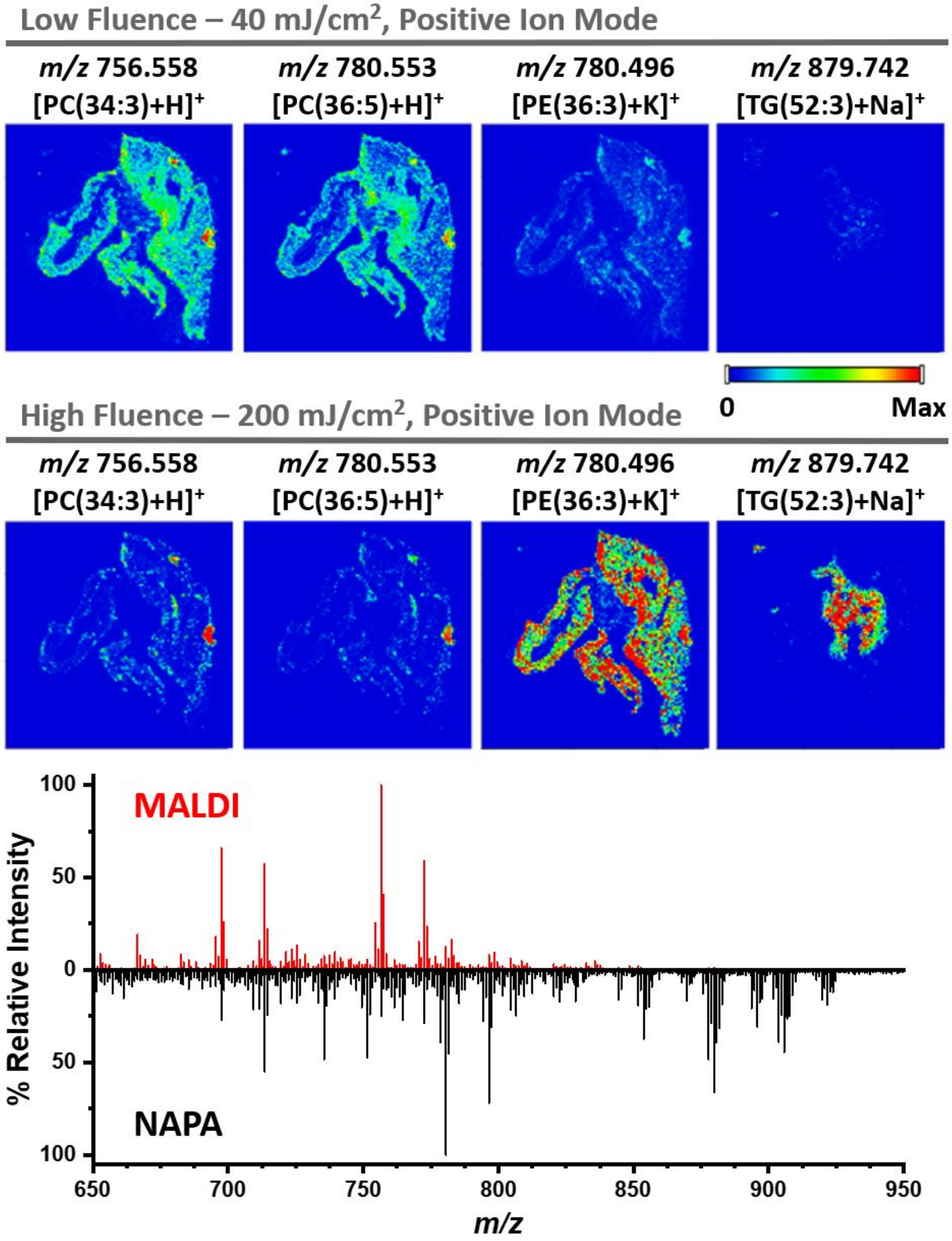

Figure 3. Images showing ion intensity distributions throughout a section of mouse lung tissue. Images in the top row were generated by a low laser fluence (40 mJ/cm^2) MALDI pass, whereas images in the middle row were generated by a high laser fluence (200 mJ/cm^2) NAPA pass. All data was collected in positive ion mode. Acquisitions were performed consecutively on the same tissue section. The bottom panel shows the comparison of mass spectra averaged over approximately the entire tissue area for the MALDI- and NAPA-LDI-MSI acquisitions.

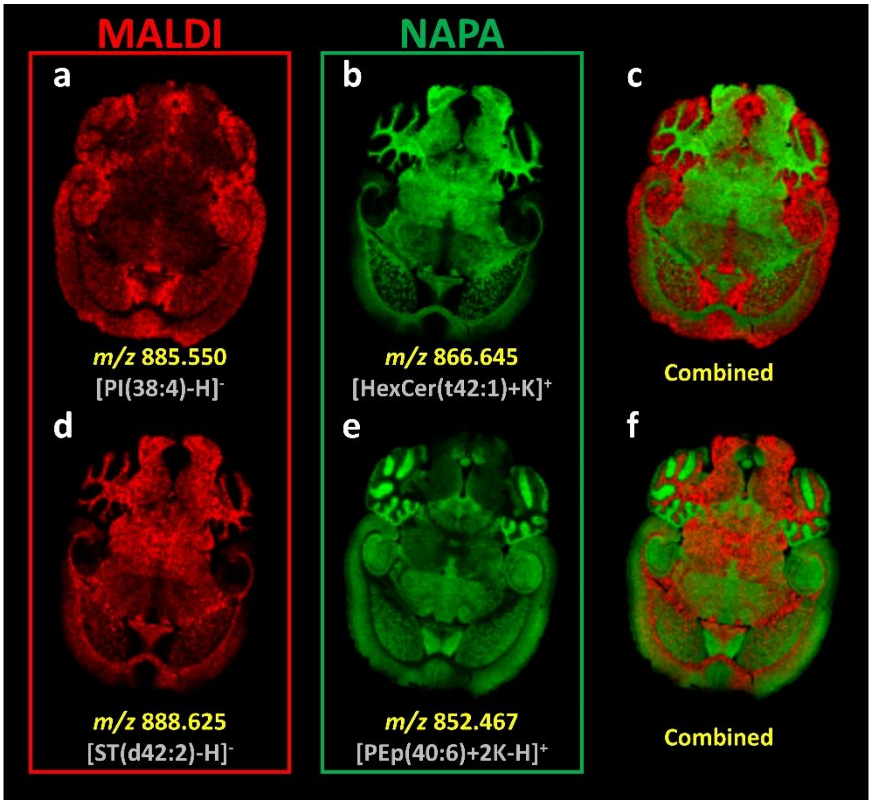

Figure 4. Overlaid chemical images from consecutive MALDI- and NAPA-LDI-MSI analysis of the same mouse brain tissue section. Images were overlaid using ImageJ software.

Table of contents entry

Sequential imaging of a tissue section by MALDI and NAPA-LDI mass spectrometry provides enhanced molecular coverage.

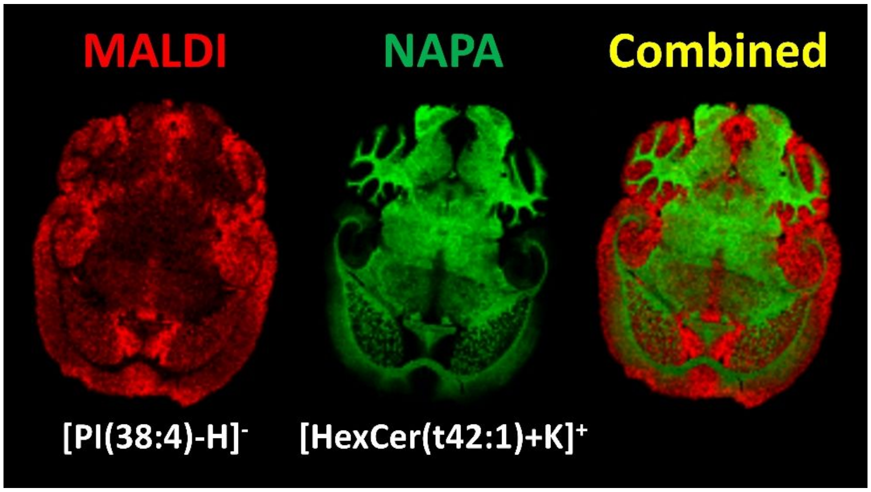

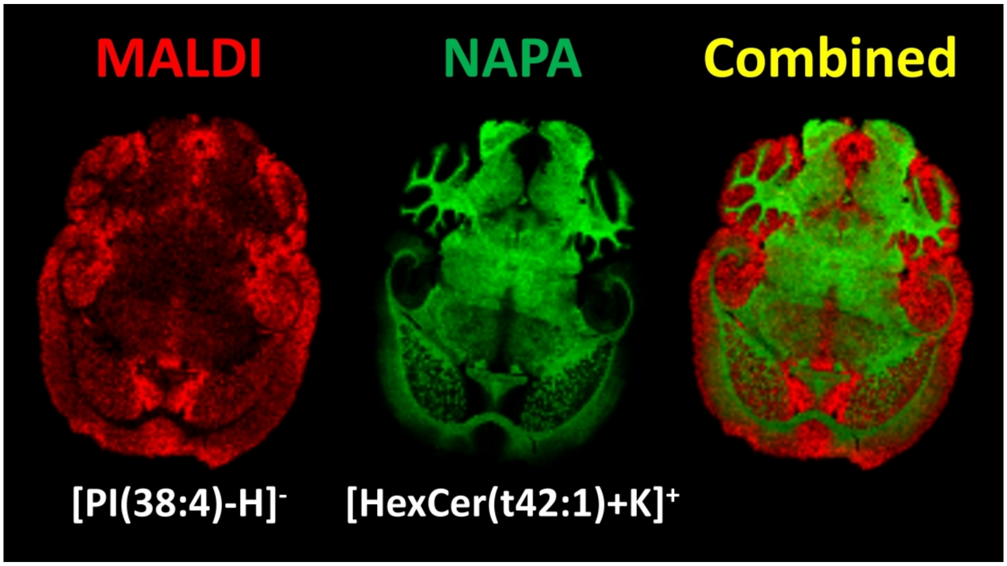

1020x571mm (96 x 96 DPI)